IEEE Photonics Journal
An IEEE Photonics Society Publication

Open Access

Broadband Terahertz Polarizing Beam Splitter Based on a Graphene-Based Defective One-Dimensional Photonic Crystal

Volume 11, Number 5, October 2019

Ziba Saleki
Yurui Fang
Samad Roshan Entezar

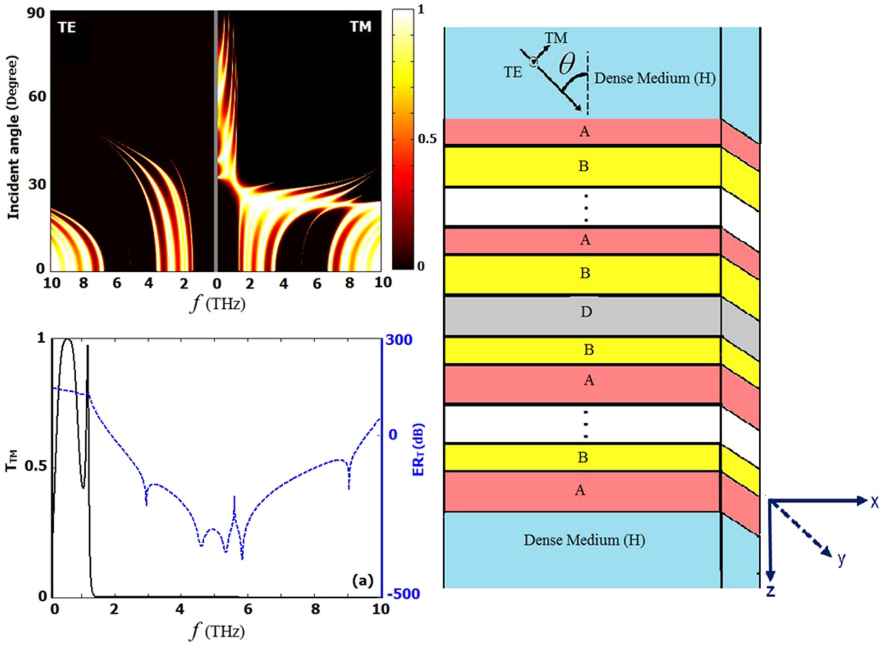

DOI: 10.1109/JPHOT.2019.2935084

Broadband Terahertz Polarizing Beam Splitter Based on a Graphene-Based Defective One-Dimensional Photonic Crystal

Ziba Saleki,[1] **Yurui Fang**,[1] **and Samad Roshan Entezar** [2]

[1]Key Laboratory of Materials Modification by Laser, Electron, and Ion Beams (Ministry of Education), School of Physics, Dalian University of Technology, Dalian 116024, China
[2]Faculty of Physics, University of Tabriz, Tabriz 5167618949, Iran

DOI:10.1109/JPHOT.2019.2935084

Manuscript received July 29, 2019; accepted August 8, 2019. Date of publication August 19, 2019; date of current version August 27, 2019. This work was supported in part by the National Natural Science Foundations of China under Grant 11704058, and in part by the Fundamental Research Funds for the Central Universities (DUT19RC(3)007). Corresponding authors: Ziba Saleki and Yurui Fang. (e-mail: ziba_saleki@yahoo.com; yrfang@dlut.edu.cn).

This paper has supplementary downloadable material available at http://ieeexplore.ieee.org, provided by the authors.

Abstract: Seeking operative terahertz (THz) devices has always stimulated considerable attention. Of particular interest is the THz beam splitter. Here, a tunable THz polarizing beam splitter (PBS) is proposed based on a graphene-embedded quarter-wave stack with a central defect layer of air. The spectral performance of the structure is investigated by the transfer matrix method. It is found that the electromagnetic waves can be decomposed into two separate polarized waves at incident angles greater than the critical angle. Furthermore, it is shown that a new kind of Brewster angle is found at the low THz frequencies due to the existence of the graphene nano-layers. The appearance of this angle which we call it the graphene induced Brewster angle results in the separation of TM- and TE- polarized waves at the low THz frequencies ($f < 2$ THz) in addition to the high THz region. It is shown that the working frequency range of PBS can be easily tuned by adjusting the width of the defect layer of air and also by tuning the chemical potential of graphene nano-layers via a gate voltage. The analysis of the proposed PBS is confirmed by the Finite Element Method (FEM) simulations that were performed with the commercial software COMSOL 5.2. Our investigations also reveal that the high transmission extinction ratio (>200 dB) for TM waves with frequency $f < 2$ THz is achieved by increasing the chemical potential to 0.5 eV. Moreover, this structure can exhibit extremely high extinction ratio for TE waves with high THz frequencies. Finally, the degree of polarization equals to one is reported for the PBS proposed here. This structure offers the opportunity to realize a high-efficiency PBS with very high extinction ratios at the broadband THz frequency.

Index Terms: Polarizing beam-splitter, defective photonic crystal, graphene nano-layers, extinction ratio, degree of polarization

1. Introduction

Since their discovery, photonic crystals (PCs), artificially designed periodic dielectric materials, have become an indispensable technology across the entire field of optical physics because of their ability to control and confine of electromagnetic waves [1], [2]. Their periodic index modulation

leads to the generation of frequency regions known as photonic band gaps (PBGs) in which the propagation of the electromagnetic waves is forbidden [3]. This unique feature of the PCs can lead to many potential applications in photonics, including optical reflectors [4], [5], localization of photon [6], suppression of spontaneous emission [7], [8], fabrication of PC waveguides [9], [10], etc. Introducing a defect layer into a PC can result in the appearance of a localized defect mode within the PBG, which enhances the applications proposed for PCs [11]–[15].

On the other hand, each optical element used in communication devices needs at least one optically tunable instrument in modern technology. Tunable optical materials allow for proper variation of their characteristics through certain external parameters. So, it is highly appropriate to use the materials with externally controllable optical parameters in the layered structures. In recent years, graphene, a single two dimensional plane of carbon atoms arranged in a honeycomb lattice, has attracted tremendous attraction due to its impressive physical properties, including high mobility of carriers, flexibility, gate-controllable Fermi level, and extraordinary electrical properties [16]–[18]. The electronic and optical response of the graphene which is described by the frequency-dependent surface conductivity can be effectively tuned by controlling the Fermi level or the chemical potential via an electric field. Besides, the dissipative loss of the graphene is dramatically small in comparison with usual metals at the frequency ranges of THz and far-IR [19]–[21]. Due to these superior characteristics, graphene has become a most promising candidate for tunable photonic components and has opened several venues of basic science exploration [22]–[24]. So, people have been motivated to study the one dimensional (1D) multilayer structures containing graphene nano-layers. It has been shown that embedding graphene nano-layers between adjacent dielectric layers of a periodic structure, enables tailoring photonic band gaps of the structure [25]–[32].

Recently, considerable attention has been directed to the study of the PCs application as a polarizing beam splitter (PBS) due to their importance in the fields of optical communication systems, optical information processing, optical reading, fiber-optic sensors, and electro-optic detectors [33]–[40]. PBSs are used to separate two orthogonal linear polarization states (transverse electric (TE) and transverse magnetic (TM) polarizations) of light into different directions. Frequency band, reflectance or transmittance of orthogonal polarization, extinction ratio and degree of polarization are the main characteristics of PBSs. In the optical realm, a conventional PBS could be fabricated by many methods, such as multimode interference structures, grating structures, multilayer films, and metamaterials [41]–[46]. But the performance of the PBSs realized by such structures is hampered by the large sizes, scarce natural birefringent crystals, high prices and complex techniques of fabrication and existence of high metallic losses and lack of tunability properties. Tunability and the switching properties of PBS are essential features in order to extend their applications in many fields such as optical instruments, laser technology, photoelectronic display, and optical memory.

Recently, the authors proposed a defective 1D PC containing graphene nano-layers which could be used as a tunable narrowband THz filter [26]. In the mentioned paper, some interesting peculiarities of the defect modes are investigated and it is shown that the structure can support a defect mode at the graphene induced PBG for wide defect layers. In their recent works, they reported omnidirectional broadband THz filter based on a one-dimensional Thue-Morse quasiperiodic structure containing graphene nano-layers. Also, they showed that the mentioned structure can act as a polarizing beam splitter [28]. So, it is expected to gain novel results in the defective PCs containing graphene nano-layers if the input beam is incident from an optically dense medium onto the structure, unlike the previous reports.

Therefore, in the present paper, we theoretically investigate the optical properties of a graphene-based defective 1D-PC in which Si and SiO_2 are used as the high index and low index dielectric alternating layers and graphene nano-layers are embedded between adjacent dielectric layers. Investigation of the propagation of photons in this structure reveals that the presented multilayer structure may be utilized in designing PBS over a broadband THz frequency. The results indicate high extinction ratio and degree of polarization for both TM and TE-polarized wave within wide frequency and wide angle range. The paper is organized as follows: in Section 2, we present the model and the physical theory to investigate the transmission spectra of the structure using well-known transfer matrix method. Additionally, the calculated performance of the PBS will be

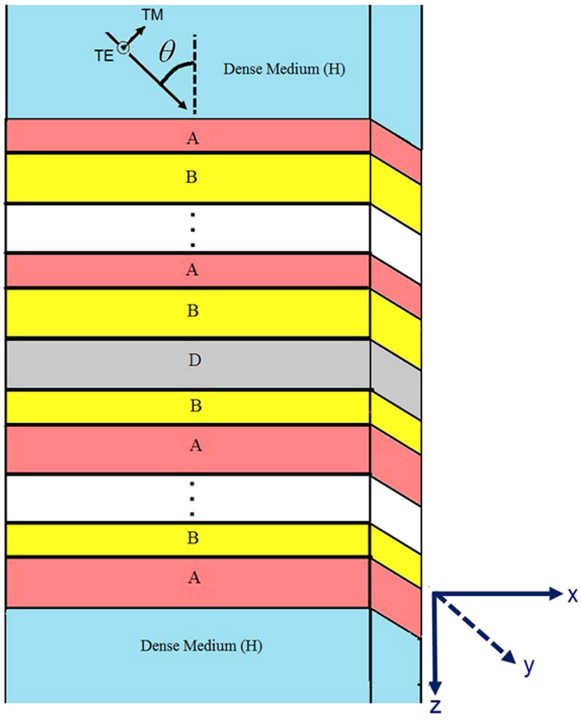

Fig. 1. (Color online) Schematic illustration of the 1D graphene-embedded defective PC with the structure $H(AGBG)^N D(GBGA)^N H$ in investigation: low index and high index dielectric layers are separated by graphene nano-layers, all are lying on the x-y plane, and light propagates along the z-direction. Here, A, B, G, and D are considered to be SiO_2, Si, graphene nano-layers, and the defect layer of air, respectively. Also, H stands for the dense medium with $n_H = 3.48$.

described. In Section 3, the general calculated results and the analysis of them are presented. We summarize the finding results in Section 4.

2. Theoretical Model

Fig. 1 illustrates a typical layout of the proposed structure, a 1D defective PC containing graphene nano-layers (G) which is expressed as $H(AGBG)^N D(GBGA)^N H$. Here, A and B represent two kinds of different isotropic dielectric layers with the thicknesses, d_A, d_B, and refractive indices, n_A, n_B, respectively. N is the PC period number. The central layer, D, denotes a defect layer of air with the thickness d_D and refractive index n_D. Here, we assumed that the layered structure is surrounded by the dense medium H with the refractive index n_H. It is known that the optical properties of the graphene nano-layer is mainly described by its refractive index $n_G = \sqrt{1 + \frac{i\sigma_G \eta_0}{k_0 d_G}}$. Here, d_G is the thickness of the graphene nano-layer, $k_0 = \frac{2\pi}{\lambda}$ is the vacuum wave vector, η_0 is the impedance of air, and σ_G is the frequency-dependent surface conductivity of graphene nano-layer which can be calculated according to the Kubo formula [47] including the intraband and interband transition contributions as $\sigma_G(\omega) = \sigma_G^{intra}(\omega) + \sigma_G^{inter}(\omega)$. Here,

$$\sigma_G^{intra} = \frac{e^2}{4\hbar}\frac{i}{2\pi}\left\{\frac{16\, k_B T}{\hbar\omega} ln\left(2\, cosh\left(\frac{\mu_c}{2k_B T}\right)\right)\right\},$$
$$\sigma_G^{inter} = \frac{e^2}{4\hbar}\left\{\frac{1}{2} + \frac{1}{\pi} arctan\frac{\hbar\omega - 2\mu_c}{2k_B T} - \frac{i}{2\pi} ln\frac{(\hbar\omega + 2\mu_c)^2}{(\hbar\omega - 2\mu_c)^2 + (2k_B T)^2}\right\}, \quad (1)$$

where, e is the charge of the electron, $\hbar$ is the reduced Planck's constant, T is the temperature in Kelvin, k_B is the Boltzmann constant and μ_c is the chemical potential which is determined by the carrier density and can be controlled either by chemical doping or by the application of a gate voltage. According to these expressions, the intraband contribution which is due to scattering processes from phonons, electrons, and impurities is important at relatively low frequencies. While the interband contribution which is due to electron-hole recombination is neglectable when $\hbar\omega$ is much smaller than the chosen chemical potential [48], [49]. We assume that the plane wave is injected from the dense medium H into the structure at an incident angle θ with respect to the Z direction. Suppose the transverse electric wave (TE), e.g., the electric field E is in the y-direction, the dielectric layers are parallel to the x–y plane and the z-direction is normal to the interface of each layer. To analyze the transmittance spectra of the structure, we use the transfer matrix method. Generally, the electric and magnetic fields at any two positions z and $z + \Delta z$ in the same layer can be related using the transfer matrix method as [50], [51]:

$$\begin{pmatrix} E(z) \\ H(z) \end{pmatrix} = M_j^{\Delta z}(\omega) \begin{pmatrix} E(z+\Delta z) \\ H(z+\Delta z) \end{pmatrix}, \tag{2}$$

where,

$$M_j^{\Delta z}(\omega) = \begin{pmatrix} \cos(k_z^j \Delta z) & -\frac{i}{q_j}\sin(k_z^j \Delta z) \\ -i q_j \sin(k_z^j \Delta z) & \cos(k_z^j \Delta z) \end{pmatrix}, j = A, B, G, D. \tag{3}$$

Here, $k_z^j = \frac{\omega}{c}\sqrt{n_j^2 - \sin^2\theta}$ is the z-component of the wave vector in the jth layer, $q_j = -\frac{k_z^j}{\omega\mu_0}$ for TE wave and $q_j = \frac{k_z^j}{\omega\varepsilon_0 n_j^2}$ for TM wave, where ε_0 and μ_0 are the permittivity and the permeability of the vacuum, respectively. Then, the transmission of the structure can be expressed as

$$T = \zeta_j \left| \frac{1}{X(1,1)} \right|^2, \tag{4}$$

where $X(1, 1)$ is the (1, 1) element of total transfer matrix $X = M_i(M_A M_G M_B M_G)^N M_D (M_G M_B M_G M_A)^N M_f$ and $\zeta_j = \frac{k_z^f}{k_z^i}$. Also, k_z^i and k_z^f are the z-component of the wave vector in the input and output media, respectively. Here, $M_i = \frac{1}{2}\begin{pmatrix} 1 & \frac{1}{q_H} \\ 1 & -\frac{1}{q_H} \end{pmatrix}$, $M_f = \begin{pmatrix} 1 \\ q_H \end{pmatrix}$, $q_H = -\sqrt{\frac{\varepsilon_0}{\mu_0}} n_H \cos\theta$ $\left(q_H = \sqrt{\frac{\mu_0}{\varepsilon_0}}\frac{\cos\theta}{n_H}\right)$ for TE (TM) waves.

3. Results

Let us now present our numerical results to illustrate the effect of graphene nano-layers and defect layer of air on the performance of the polarizing beam splitter which is constructed by the graphene-based 1D defective PC with the structure $H(AGBG)^N D(GBGA)^N H$. Our calculations are limited only to the frequency range of 0 to 10 THz due to the low loss of the graphene nano-layers in this interval. Besides, the dispersion of the usual dielectric materials is not noticeable in this region [52]. Throughout this work, the PC layers A and B are chosen to be SiO_2 and Si with the refractive indices $n_A = 1.45$, $n_B = 3.48$, respectively, and also $n_H = 3.48$. The thicknesses of two dielectric layers are considered to be $n_A d_A = n_B d_B = \frac{\lambda_0}{4}$, where λ_0 is the wavelength corresponding to the center frequency of 5 THz. The period number of the structure is taken to be $N = 4$, so the total number of layers is 9, including the defect layer of air. Also, the optical and geometrical parameters of the graphene nano-layers and defect layer are taken as: $d_G = 0.34$ nm, $\mu_c = 0.2$ eV, $T = 300$ K, $n_D = 1$.

The Finite Element Method (FEM) simulations were performed with a 2D model using commercial software COMSOL 5.2. The parameters are exactly the same as mentioned above. Floquet periodic boundary conditions were used to perform the infinity layers under tilted incident light. Port boundary conditions were used to excite the structure. Non-uniform meshes were used to finely format the layers and reduce the total freedom number.

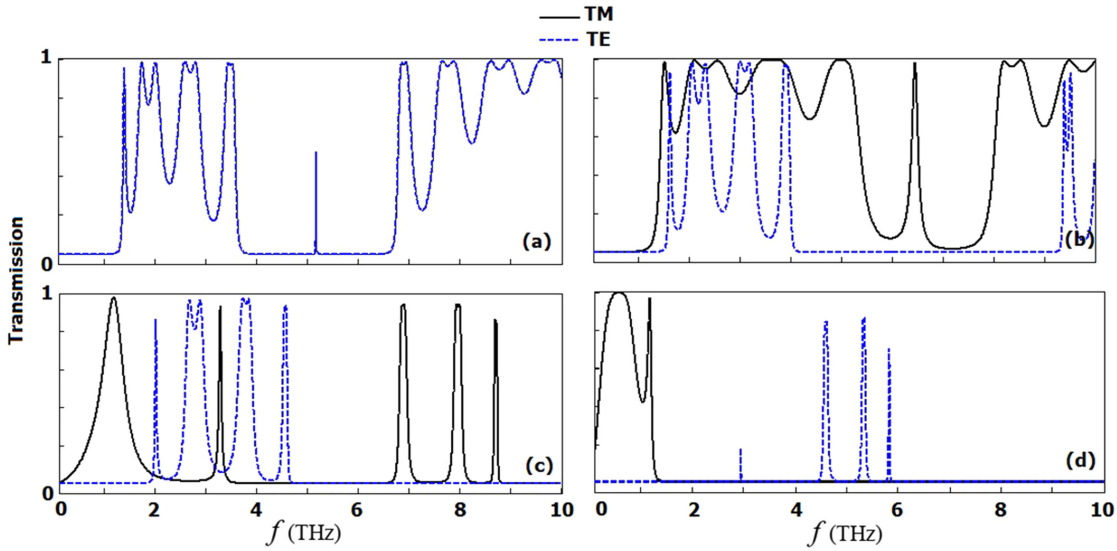

Fig. 2. (Color online) Transmission spectra of the 1D graphene-based defective PC with the structure $H(AGBG)^N(GBGA)^N H$ as functions of frequency for TM polarization (solid lines) and TE polarization (dashed lines) at different incident angles (a) 0°, (b) 20°, (c) 30°, and (d) 40°. Here, $\mu_c = 0.2$ eV.

Firstly, the optical transmission spectra of the structure $H(AGBG)^N(GBGA)^N H$ are plotted for the TM-(solid lines) and the TE-(dashed lines) polarized waves in Figs. 2(a)–(d) at some specific values of the incident angles 0°, 20°, 30°, and 40°, respectively. Here, the width of the air defect layer is considered to be $d_D = 0$. The figure shows that the structure contains two band gaps at the desired frequency range at the normal incidence case (see Figs. 2(a)). The first gap (around 1 THz) is a GIPBG [26] which is created due to the joint contribution of graphene conductance and Bragg scatterings of the dielectric stack and the second gap (around 5 THz) is a conventional Bragg gap. As one can see the position and width of the band gaps are substantially modified by increasing the incident angle θ. This feature is more pronounced in the Bragg gap compared to the GIPBG. Figs. 2(a)–(d) reveal that by increasing the incident angle θ, the structure shows a wider GIPBG and also wide Bragg gap with some resonant transmission lines for TE-polarized wave, whereas, in the case of the TM-polarized wave, the GIPBG becomes narrower and it is finally replaced by some resonant transmission peaks, which is confirmed by FEM numerical simulations (Figs. 3 and supporting information). Based on this behavior, some of the resonant frequencies are transmitted for one of the polarizations, while for the other polarization the transmittance of the structure reaches nearly to zero at incident angles greater than the critical angle. The different behaviors of TM- and TE-polarized waves allow us to utilize this device as a polarizing beam splitter at the broadband interval of THz frequencies.

One can determine that the electric field in the layers SiO_2 at $\theta > 24.6°$ and also at $\theta > 16.7°$ in the air defect layer for our selected parameters is caused by the Bragg reflection. So, the appeared resonant transmission lines at incident angles greater than the critical angle (see Figs. 2(c)–(d)) are due to the interaction of the Bragg reflection in the low index and the high index layers.

To further investigate the GIPBG and other effects, the electric near field distributions and surface currents were simulated with FEM as shown in Fig. 3. Several typical frequencies at the band gaps and transmission peaks are chosen to show the difference. The first one shown in part (i) of Fig. 3(b) is the GIPBG. As one can see that when there is no graphene layers, there is strong transmission corresponding to the Fabry-Perot (FP) condition. However, when the graphene layers existing between the interfaces, induced surface currents appear on graphene layers, which changes the periodic conditions of the photonic crystal and there is new band gap so called GIPBG. From Fig. 3(b), part (ii) we can see that the band gap between 4 THz and 6.5 THz is

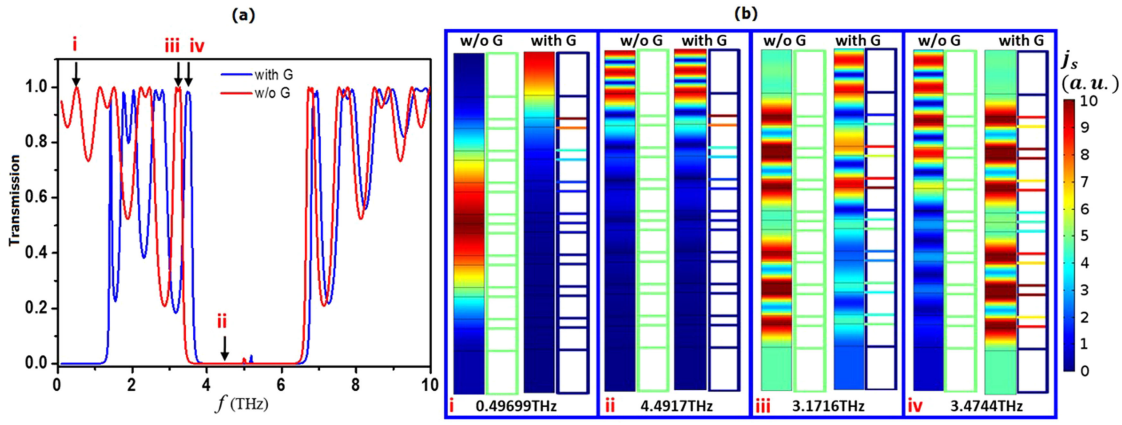

Fig. 3. (Color online) FEM simulations with the same parameters with Fig. 2a. (a) The transmission with and without graphene layers. (b) The near electric field intensity at the frequency (left surface slices) indicated in a and corresponding surface current j_s (right line frames) with and without graphene, respectively.

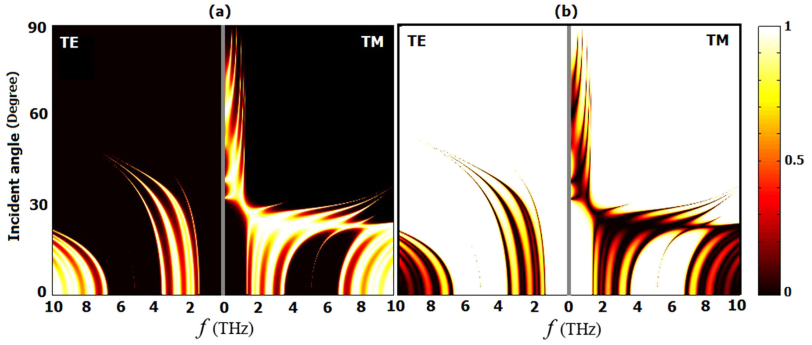

Fig. 4. (Color online) (a) Transmission spectra, (b) reflection spectra of the 1D graphene-based defective PC with the structure $H(AGBG)^N(GBGA)^N H$ in the plane of (f, θ) for TM polarization (right panel) and TE polarization (left panel). Here, $\mu_c = 0.2$ eV.

just blue shifted because of the graphene surface current. Because the band gap exists without graphene layers, so people don't call it GIPBG even if there is graphene effect. Fig. 3(b) (iii) shows that without graphene, there is transmission maximum at 3.1716 THz, which is the FP effect and shows symmetric electric field distribution with the defect layer as well as other transmission peaks. When the graphene layers are added, the induced surface current causes a FP minimum transmission condition. Opposite condition happens at 3.4744 THz shown as Fig. 3(b), part (iv). The FEM simulated polarization-dependent transmissions under different incident angles for TE and TM polarized waves corresponding to Fig. 2 show quite well agreement with the theoretical model (Fig. S1). Furthermore, the electric field distributions and the surface current at the graphene boundaries show very similar behavior to the illustration above. When there is a transmission peak, the electric field will spread in the whole structure with the periodic medium distributions.

To further clarify the angular dependence of the designed PBS, the transmission and reflection spectra of the structure $H(AGBG)^N(GBGA)^N H$ are plotted as functions of incident angle and frequency for TM- (right panel) and TE- (left panel) polarized waves in Figs. 4(a)–(b), respectively. In Fig. 4(a), white (black) color represents a transmission coefficient equal to 1 (0) corresponding to the colour legend band next to the figure. As it is obvious from the figure, the results are in a good agreement with the formerly mentioned ones, and other useful information can be obtained from them; GIPBG which is induced in the low-frequency region (0–1.5 THz) due to the presence

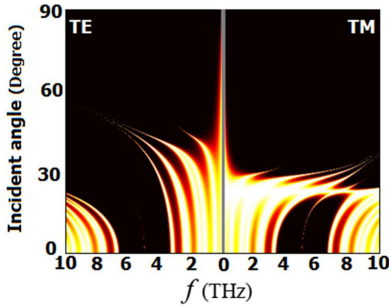

Fig. 5. (Color online) Transmission spectra of the graphene-based 1D defective PC with the structure $H(AB)^N(BA)^N H$ in the plane of (f, θ) for TM polarization (right panel) and TE polarization (left panel). Here, $\sigma_G = 0$ and the other parameters are the same as those of Fig. 4.

of the graphene nano-layers between the dielectric layers disappears for incident angles greater than 30 degree for TM-polarized wave, in other words, there is a range of incident angle for which the transmission of the structure is almost zero for TE-polarized waves at the frequency region 0–1.5 THz while TM-polarized waves are transmitted completely at the same frequency region. Notice that the constituent layers of the 1D PC are lossless and the graphene nano-layers absorption is negligible in this domain. Moreover, Fig. 4(b) certifies that the TE-polarized waves at the mentioned frequency region will be reflected completely. Here, the white (black) color stands for a reflection coefficient equal to 1 (0). Since this behavior is appeared because of the existence of the graphene nano-layers in the structure, we can call this angle ($\theta \cong 30^\circ$) as a graphene induced Brewster angle at low THz frequencies. The results imply that if a mixed-polarized wave with a frequency between 0 and 1.5 THz is incident from the optically dense medium into the structure at an angle greater than induced Brewster angle, TE and TM waves can be split.

In order to identify how the function of PBS is affected by the graphene nano-layers, we plotted the transmission spectra of the structure in the absence of graphene nano-layers (i.e.,$H(AB)^N(BA)^N H$) for TM- (right panel) and TE- (left panel) polarized waves at the plane of (f, θ) in Fig. 5. As one can see from Fig. 5, the GIPBG is disappeared for both TE and TM cases. Comparing these results with Fig. 4(a) reveals that in the existence of graphene nano-layers, the proposed structure can act as a polarizing beam splitter not only at high THz domain but also at the low THz frequencies (0–1.5 THz) for incident angle greater than induced Brewster angle. Therefore, this periodic structure offers the opportunity to achieve a polarizing beam splitter to separate TM- and TE-polarized modes at the low THz frequencies in addition to the high THz frequencies. This different behavior of the structure at low THz frequencies can be explained from the fact that the presence of the graphene nano-layers modifies the interference conditions which can affect the behavior of the bandgaps.

As we know, the optical characteristics of graphene nano-layer which is dependent on its surface conductivity can be varied by tuning the chemical potential. Therefore, the optical response of the structure and also the effective frequency domain of PBS can be tuned by the controlling parameter such as chemical potential μ_c via an external gate voltage. In the experimental realization, this voltage can be provided by electrodes which are THz-transparent dc conductors, such as thin-doped InSb films [53], [54].

Hence, we are interested in checking how the PBS behaves when changing the chemical potential. To show this, the transmission spectra of the structure $H(AGBG)^N(GBGA)^N H$ are plotted in Figs. 6(a)–(b) for TM- (right panel) and TE- (left panel) polarized waves at the incident angles 30° and 40° respectively, in the plane of (μ_c, f). The figures reveal that the frequency of the resonant transmission peaks and operating frequency interval of PBS can be effectively tuned in wide limits by adjusting the chemical potential via an external gate voltage. So, one may conclude that the mentioned structure would have optimum potential applications in designing PBS for incident angles greater than induced Brewster angle.

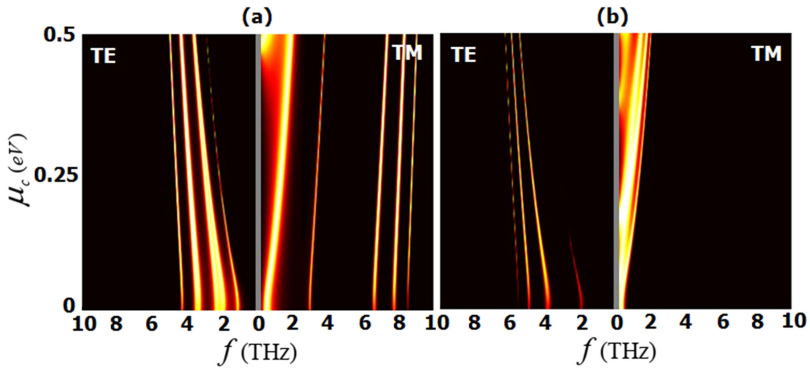

Fig. 6. (Color online) Transmission spectra of the 1D graphene-based defective PC with the structure $H(AGBG)^N(GBGA)^N H$ in the plane of (f, μ_c) for TM polarization (right panel) and TE polarization (left panel) at the incident angle (a) $\theta = 30^\circ$ and (b) $\theta = 40^\circ$.

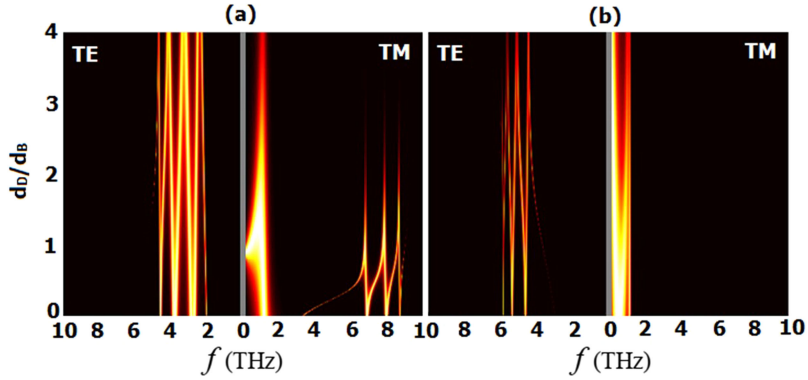

Fig. 7. (Color online) Transmission spectra of the 1D graphene-based defective PC with the structure $H(AGBG)^N(GBGA)^N H$ in the plane of (f, $\frac{d_D}{d_B}$) for TM polarization (right panel) and TE polarization (left panel) at the incident angle (a) $\theta = 30^\circ$ and (b) $\theta = 40^\circ$. Here, $\mu_c = 0.2$ eV.

In the next stage, we would like to investigate how the working frequency range of the PBS can be tuned simply by adjusting the width of the air defect layer. To show this, we examine the case of $H(AGBG)^N D(GBGA)^N H$. Figs. 7(a)–(b) displays the transmission spectra of the structure $H(AGBG)^N D(GBGA)^N H$ in the plane of (f, $\frac{d_D}{d_B}$) for TM- (right panel) and TE- (left panel) polarized waves at the incident angles 30° and 40°, respectively. As Fig. 7 reveals that we can adjust the operating frequency domain of PBS by tuning of the thickness of the defect layer of air at the given incident angle.

Next, we will focus on the important performance parameter of the PBS, transmission extinction ratio (ER_T), which can be defined as

$$ER_T = 10 \log \left(\frac{T_{TM}}{T_{TE}} \right), \tag{5}$$

Here, T_{TM} and T_{TE} denotes the transmission coefficients for the TM- and TE-polarized waves, respectively. Based on Equation (5), the extinction ratio is sensitive to slight decrease in T_{TE}. Thus T_{TE} should be very low to obtain high transmission extinction ratio for TM-polarized wave. In Figs. 8(a)–(b) the transmission intensity T_{TM} of the PBS for the TM- polarized wave and also calculated ER_T are shown versus the frequency at the incident angle 40° (a) in the presence and (b) in the absence of graphene nano-layers. All the other parameters are kept constant. It is evident from Fig. 8(a) that the ER_T reaches above 130 dB in the frequency range from 0 to 1.5 THz.

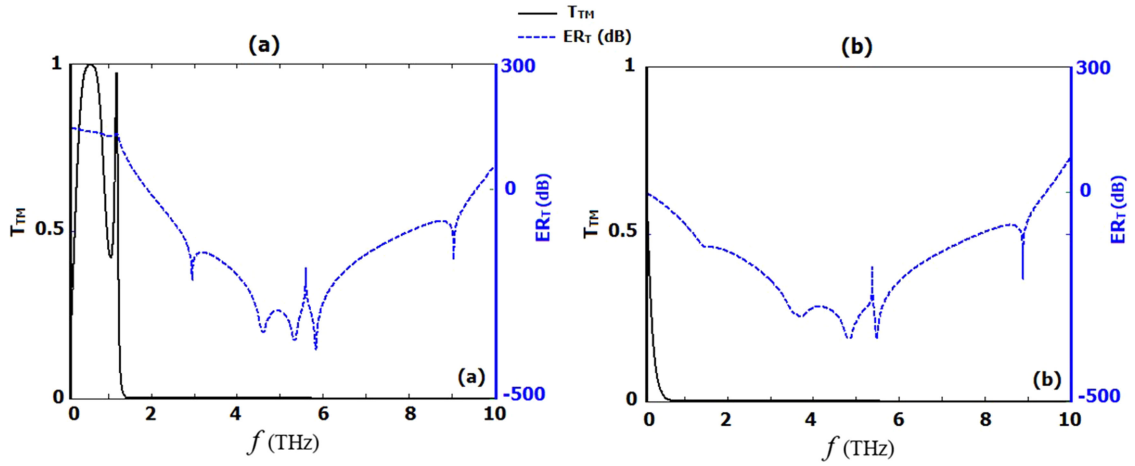

Fig. 8. (Color online) Transmission intensities (solid lines) and transmission extinction ratios (dashed lines) of the structure (a) $H(AGBG)^N(GBGA)^N H$ and (b) $H(AB)^N(BA)^N H$ as a function of frequency for TM-polarized wave at the incident angle $\theta = 40^\circ$.

High values of ER_T at $f < 1.5$ THz clarify that when the mixed TE/TM polarized wave is injected from the dense medium to the structure, the TM-polarized wave transmits through the structure, while the transmission of TE-polarized wave is nearly zero. Moreover, high negative values for ER_T at high THz frequencies declare that the structure is completely transparent for TE-polarized waves and acts as an almost perfect reflective mirror for TM-polarized waves at the wide range of THz frequency. Therefore near-ideal broadband polarizer is possible at the THz region. Since the graphene nano-layers have a leading role at the relatively low frequencies, it may be anticipated that the exist of graphene nano-layers in the structure can affect the ER_T around the low THz frequencies. As it is clear from Fig. 8(b) ER_T of the structure without graphene nano-layers keeps almost zero at the range of low frequencies. Comparing the results of Fig. 8(a) with Fig. 8(b) reveals that the transmittance of the TM-polarized wave and hence the ER_T is dramatically improved at the low THz frequencies, in the presence of graphene nano-layers. Therefore, excellent performance is concluded when graphene nano-layers are considered between dielectric layers of the PC.

As mentioned before, the surface conductivity of graphene nano-layer depends on its chemical potential. Therefore, changing the chemical potential of the graphene nano-layer via an external gate voltage may render the possibility of controlling the transmission spectrum, and then offer tunability of ER_T. To show this, the transmission extinction ratio of the structure $H(AGBG)^N(GBGA)^N H$ is plotted as a function of frequency in Fig. 9 for three different values of $\mu_c = 0.2, 0.35$ eV and 0.5 eV at the incident angle 40°. The figure clearly indicates that ER_T is considerably increased by increasing the chemical potential of the graphene nano-layers at the low THz frequencies. It is obvious that the extinction ratio exceeds 200 dB at the frequency range of 0–2 THz when the chemical potential is 0.5 eV. However, ER_T slightly depends on the chemical potential variation at the high THz region. It is interesting to notice from Fig. 9 that we can adjust the transmission extinction ratio of the structure and also the frequency of resonant transmission peaks by tuning the chemical potential via an external electric field. Hence, one may conclude that the suggested structure can operate as an efficient tunable PBS at THz frequency domain.

As we know, one of the key parameters which may affect the optical response of the 1D defective layered structures is the width of the defect layer. So, we would like to analyze how ER_T behaves when changing the width of the defect layer. To show this, the tuning trend of ER_T versus the frequency is plotted in Fig. 10, for different values of the width of the air defect layer (d_D) at the incident angle 40° and the chemical potential 0.2 eV. The figure clearly indicates that the ER_T changes minimally with the thickness of the air defect layer at the low THz frequencies. However,

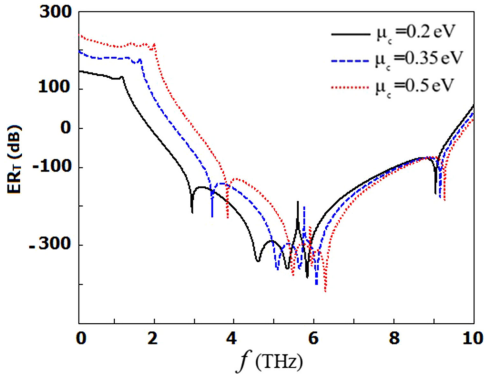

Fig. 9. (Color online) Transmission extinction ratios of the structure $H(AGBG)^N(GBGA)^N H$ as a function of frequency at the incident angle $\theta = 40^\circ$ for different chemical potential values: $\mu_c = 0.2$, 0.35 eV, and 0.5 eV (solid, dashed, and dotted lines, respectively).

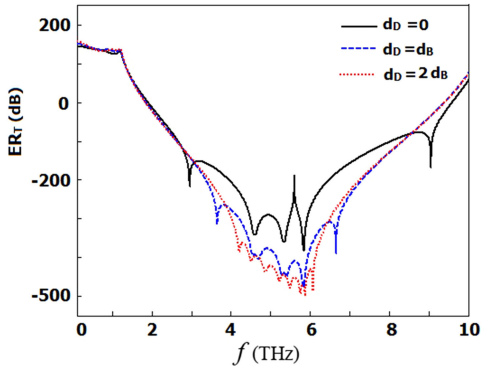

Fig. 10. (Color online) Transmission extinction ratios of the structure $H(AGBG)^N D(GBGA)^N H$ as a function of frequency at the incident angle $\theta = 40^\circ$ and chemical potential $\mu_c = 0.2$ eV with $d_D = 0$ (solid line), $d_D = d_B$ (dashed line), and $d_D = 2d_B$ (dotted line).

the absolute value of ER_T experiences a considerable increase by increasing the defect layer width at the high THz region. Also, it is observed that the extinction ratio can reach the highest value, which is 499 dB, when the frequency is 5.88 THz and $d_D = 2d_B$. From an optical engineering viewpoint, it is useful to implement some tools to tune the key features of PBS. Thus, by comparing Fig. 9 with Fig. 10 one may conclude the following tuning properties for the presented graphene-based PBS:

i)The ER_T parameter of PBS exhibits a conspicuous tuning trend with chemical potential of graphene nano-layer at the low THz region. This result is in agreement with the previous result of Fig. 8 that represents the graphene nano-layer has an operative effect on the optical response of the structure at low THz frequencies. Also, it is needed to increase the chemical potential of graphene nano-layers to reach the highest value of ER_T in order to optimally design of graphene-based PBS.

ii)The notable increase of ER_T parameter at high THz region can be obtained by increasing the width of air defect layer. Moreover, the working frequency of the PBS may be tuned easily by adjusting the width of the air defect layer.

For the sake of completeness, let us briefly discuss the other essential feature of PBS, i.e. efficiency of PBS. The efficiency of PBS is characterized by its degree of polarization, P, which is defined by [55], [56].

$$P = \left| \frac{T_{TM} - T_{TE}}{T_{TM} + T_{TE}} \right|, \tag{6}$$

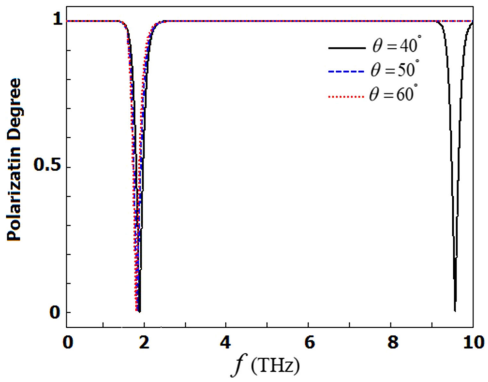

Fig. 11. (Color online) Degree of polarization of THz wave transmits through the structure $H(AGBG)^N(GBGA)^N H$ as a function of frequency at the incident angle $\theta = 40^\circ$ (solid line), $\theta = 50^\circ$ (dashed line), and $\theta = 60^\circ$ (dotted line). Here, $\mu_c = 0.2$ eV.

where T_{TM} and T_{TE} are spectral transmittance for TM- and TE-polarized waves, respectively. For an ideal PBS, P equals to 1, according to Eq. (6). Fig. 11 shows the degree of polarization of our PBS as a function of frequency at various incident angles. Here, $\mu_c = 0.2$ eV, $d_D = 0$. It is easily seen that $P = 1$ is achieved for $f < 1.5$ THz and $2.45 < f < 9.2$ THz at the incident angle 40°. It is apparent that the frequency range in which the degree of polarization equals to 1 is broadened by increasing the incident angle. Then, the graphene-based PBS proposed here has almost 100% efficiency at the wide range of THz frequency $f < 1.5$ THz and also $2.45 < f < 10$ THz as indicated in Fig. 11. Our findings indicate that the proposed PBS can split TM- and TE-polarized waves into different propagation directions with very high efficiency over broadband THz frequencies. It's worth noting that, the proposed structure in Ref. [28] also could be used as a PBS. But the application of that structure as a PBS had only been shown at specific incident angles. Here, the structure has changed to a defective PC with a tunable air defect layer in which the extra essential parameters of PBS such as the polarization degree and the transmission extinction ratio have been reported. It is shown that the extinction ratio can reach the highest value of 499 dB and the degree of polarization equals to 1 at the wide range of THz frequency.

4. Conclusions

In summary, a novel design of a THz PBS based on a defective 1D PC containing graphene nano-layers is theoretically proposed. From the numerical results performed by the transfer matrix method, it is found that this periodic structure can act as a PBS at the low THz frequencies in addition to the high THz frequencies. The main characteristics of the proposed PBS such as the working frequency range, the extinction ratio and the degree of polarization can be finely tuned by adjusting two external controlling parameters: the width of the air defect layer and the chemical potential of the graphene nano-layers. Also, the simulations performed with the commercial software COMSOL 5.2. confirmed the obtained results. The transmitted extinction ratio can exceed 200 dB in the frequency range 0–2 THz for the TM-polarized wave if the incident angle is greater than the induced Brewster angle. Whereas the transmitted extinction ratio for the TE-polarized wave is very high at frequency region $f > 2$ THz. Finally, the high polarization efficiency can be obtained by optimization of the designed structure. A unique aspect of our work is the application of a continuously tunable THz frequency domain PBS with high ER_T and also the high degree of polarization.

References

[1] E. Yablonovitch "Inhibited spontaneous emission in solid-state physics and electronics," *Physical Rev. Lett.*, vol. 58, no. 20, 1987, Art. no. 2059.

[2] J. D. Joannopoulos, S. G. Johnson, J. N. Winn, and R. D. Meade, Photonic Crystals: Molding the Flow of Light, Princeton, NJ, USA: Princeton Univ. Press, 2011.

[3] J. D. Joannopoulos, P. R. Villeneuve, and S. Fan, "Photonic crystals: Putting a new twist on light," *Nature*, vol. 386, no. 6621, pp. 143–149, 1997.

[4] D. N. Chigrin, A. V. Lavrinenko, D. A. Yarotsky, and S. V. Gaponenko, "Observation of total omnidirectional reflection from a one-dimensional dielectric lattice," *Appl. Phys. A, Mater. Sci. Process.*, vol. 68, no. 1, pp. 25–28, 1999.

[5] C. J. Wu, B. H. Chu, and M. T. Weng, "Analysis of optical reflection in a chirped distributed Bragg reflector," *J. Electromagn. Waves Appl.*, vol. 23, no. 1, pp. 129–138, 2009.

[6] J. Topolancik, B. Ilic, and F. Vollmer, "Experimental observation of strong photon localization in disordered photonic crystal waveguides," *Physical Rev. Lett.*, vol. 99, no. 25, 2007, Art. no. 253901.

[7] F. Bordas, M. J. Steel, C. Seassal, and A. Rahmani, "Confinement of band-edge modes in a photonic crystal slab," *Opt. Express*, vol. 15, no. 17, pp. 10890–10902, 2007.

[8] V. M. Rao and S. Hughes, "Single quantum-dot Purcell factor and β factor in a photonic crystal waveguide," *Physical Rev. B*, vol. 75, no. 20, 2007, Art. no. 205437.

[9] P. Kramper *et al.*, "Highly directional emission from photonic crystal waveguides of subwavelength width," *Physical Rev. Lett.*, vol. 92, no. 11, 2004, Art. no. 113903.

[10] B. Temelkuran and E. Ozbay, "Experimental demonstration of photonic crystal based waveguides," *Appl. Phys. Lett.*, vol. 74, no. 4, pp. 486–488, 1999.

[11] J. Li, T. Tang, L. Luo, and J. Yao, "Enhancement and modulation of photonic spin Hall effect by defect modes in photonic crystal with graphene," *Carbon*, vol. 134, pp. 293–300, 2018.

[12] A. E. Miroshnichenko, I. Pinkevych, and Y. S. Kivshar, "Tunable all-optical switching in periodic structures with liquid-crystal defects," *Opt. Express*, vol. 14, no. 7, pp. 2839–2844, 2006.

[13] H. C. Hung, C. J. Wu, and S. J. Chang, "Terahertz temperature-dependent defect mode in a semiconductor-dielectric photonic crystal," *J. Appl. Phys.*, vol. 110, no. 9, 2011, Art. no. 093110.

[14] Y. K. Ha *et al.*, "Tunable omnidirectional reflection bands and defect modes of a one-dimensional photonic band gap structure with liquid crystals," *Appl. Phys. Lett.*, vol. 79, no. 1, pp. 15–17, 2001.

[15] R. Amri *et al.*, "Photonic band gap and defect mode of one-dimensional photonic crystal coated from a mixture of (HMDSO, N2) layers deposited by PECVD," *Superlattices Microstruct.*, vol. 104, pp. 298–307, 2017.

[16] A. K. Geim, "Graphene: Status and prospects," *Science*, vol. 324, no. 5934, pp. 1530–1534, 2009.

[17] F. Bonaccorso, Z. Sun, T. Hasan, and A. C. Ferrari, "Graphene photonics and optoelectronics," *Nature Photon.*, vol. 4, no. 9, pp. 611–622, 2010.

[18] K. S. Novoselov *et al.*, "Two-dimensional gas of massless Dirac fermions in graphene," *Nature*, vol. 438, no. 7065, pp. 197–200, 2005.

[19] M. Esquius-Morote, J. S. Gomez-Di, and J. Perruisseau-Carrier, "Sinusoidally modulated graphene leaky-wave antenna for electronic beamscanning at THz," *IEEE Trans. THz Sci. Technol.*, vol. 4, no. 1, pp. 116–122, Jan. 2014.

[20] C. S. Kaipa, A. B. Yakovlev, G. W. Hanson, Y. R. Padooru, F. Medina, and F. Mesa, "Enhanced transmission with a graphene-dielectric microstructure at low-terahertz frequencies," *Physical Rev. B*, vol. 85, no. 24, 2012, Art. no. 245407.

[21] G. W. Hanson, "Quasi-transverse electromagnetic modes supported by a graphene parallel-plate waveguide," *J. Appl. Phys.*, vol. 104, 2008, Art. no. 084314.

[22] C. H. Costa, L. F. Pereira, and C. G. Bezerra, "Light propagation in quasiperiodic dielectric multilayers separated by graphene," *Physical Rev. B*, vol. 96, no. 12, 2017, Art. no. 125412.

[23] L. A. Bian, P. Liu, and G. Li, "Design of tunable devices using one-dimensional Fibonacci photonic crystals incorporating graphene at terahertz frequencies," *Superlattices Microstruct.*, vol. 98, pp. 522–534, 2016.

[24] O. L. Berman, V. S. Boyko, R. Y. Kezerashvili, A. A. Kolesnikov, and Y. E. Lozovik, "On transmittance and localization of the electromagnetic wave in two-dimensional graphene-based photonic crystals," *Phys. Lett. A*, vol. 382, no. 31, pp. 2075–2080, 2018.

[25] Y. Fan, Z. Wei, H. Li, H. Chen, and C. M. Soukoulis, "Photonic band gap of a graphene-embedded quarter-wave stack," *Physical Rev. B*, vol. 88, no. 24, 2013, Art. no. 241403.

[26] S. R. Entezar, Z. Saleki, and A. Madani, "Optical properties of a defective one-dimensional photonic crystal containing graphene nanaolayers," *Physica B, Condensed Matter*, vol. 478, pp. 122–126, 2015.

[27] H. Hajian, A. Ghobadi, B. Butun, and E. Ozbay, "Tunable, omnidirectional, and nearly perfect resonant absorptions by a graphene-hBN-based hole array metamaterial," *Opt. Express*, vol. 26, no. 13, pp. 16940–16954, 2015.

[28] Z. Saleki, S. R. Entezar, and A. Madani, "Omnidirectional broadband THz filter based on a one-dimensional Thue-Morse quasiperiodic structure containing graphene nanolayers," *J. Nanophoton.*, vol. 10, no. 3, 2016, Art. no. 036010.

[29] Z. Saleki, S. R. Entezar, and A. Madani, "Optical properties of a one-dimensional photonic crystal containing a graphene-based hyperbolic metamaterial defect layer," *Appl. Opt.*, vol. 56, no. 2, pp. 317–323, 2017.

[30] J. Fu, W. Chen, and B. Lv, "Tunable defect mode realized by graphene-based photonic crystal," *Phys. Lett. A*, vol. 380, no. 20, pp. 1793–1798, 2016.

[31] A. Madani and S. R. Entezar, "Tunable enhanced Goos-Hanchen shift in one dimensional photonic crystals containing graphene monolayers," *Superlattices Microstruct.*, vol. 86, pp. 105–110, 2015.

[32] F. U. Y. Al-Sheqefi and W. Belhadj, "Photonic band gap characteristics of one-dimensional graphene-dielectric periodic structures," *Superlattices Microstruct.*, vol. 88, pp. 127–138, 2015.

[33] H. K. Khanfar and R. M. A. Azzam, "Broadband IR polarizing beam splitter using a subwavelength-structured one-dimensional photonic-crystal layer embedded in a high-index prism," *Appl. Opt.*, vol. 48, no. 27, pp. 5121–5126, 2009.

[34] M. F. Lu, S. M. Liao, and Y. T. Huang, "Ultracompact photonic crystal polarization beam splitter based on multimode interference," *Appl. Opt.*, vol. 49, no. 4, pp. 724–731, 2010.
[35] M. Lin, X. Jin, Z. Ouyang, G. Zheng, and G. Wen, "Y-type polarization beam splitter based on polarization-selective defects within crystal waveguides in a square-lattice photonic crystal with solid rods," *Chin. Opt. Lett.*, vol. 13, 2015, Art. no. s11301.
[36] L. Gong *et al.*, "Optical orbital-angular-momentum-multiplexed data transmission under high scattering," *Light, Sci. Appl.*, vol. 8, no. 1, 2019, Art. no. 27.
[37] H. X. Xu *et al.*, "Wavenumber-splitting metasurfaces achieve multichannel diffusive invisibility," *Adv. Opt. Mater.*, vol. 6, no. 10, 2018, Art. no. 1800010.
[38] J. Hou, L. Wang, C. Yang, B. Wang, and S. Chen, "Compact high extinction ratio asymmetric polarization beam splitter of periodic rods waveguide," *Appl. Opt.*, vol. 54, no. 34, pp. 10277–10282, 2015.
[39] J. Wang *et al.*, "A tunable polarization beam splitter based on magnetic fluids-filled dual-core photonic crystal fiber," *IEEE Photon. J.*, vol. 9, no. 1, Feb. 2017, Art. no. 2200410.
[40] J. Shi, M. E. Pollard, C. A. Angeles, R. Chen, J. C. Gates, and M. D. Charlton, "Photonic crystal and quasi-crystals providing simultaneous light coupling and beam splitting within a low refractive-index slab waveguide," *Scientific Rep.*, vol. 7, no. 1, 2017, Art. no. 1812.
[41] K. Yang, X. Long, Y. Huang, and S. Wu, "Design and fabrication of ultra-high precision thin-film polarizing beam splitter," *Opt. Commun.*, vol. 284, no. 19, pp. 4650–4653, 2011.
[42] H. Guan *et al.*, "Optimization design of polarizing beam splitter based on metal-multilayer dielectric reflecting grating," *Opt. Commun.*, vol. 287, pp. 25–30, 2013.
[43] M. Wei *et al.*, "Broadband non-polarizing terahertz beam splitters with variable split ratio," *Appl. Phys. Lett.*, vol. 111, no. 7, 2017, Art. no. 071101.
[44] J. Kim *et al.*, "Ultrabroadband beam splitter with matched group-delay dispersion," *Opt. Lett.*, vol. 30, no. 12, pp. 1569–1571, 2005.
[45] Z Wang, Y. Tang, L. Wosinski, and S. He, "Experimental demonstration of a high efficiency polarization splitter based on a one-dimensional grating with a Bragg reflector underneath," *IEEE Photon. Technol. Lett.*, vol. 22, no. 21, pp. 1568–1570, Nov. 2010.
[46] M. Farmahini-Farahani and H. Mosallaei, "Birefringent reflectarray metasurface for beam engineering in infrared," *Opt. Lett.*, vol. 38, no. 4, pp. 462–464, 2013.
[47] L. A. Falkovsky and S. S. Pershoguba, "Optical far-infrared properties of a graphene monolayer and multilayer," *Physical Rev. B*, vol. 76, no. 15, 2007, Art. no. 153410.
[48] L. A. Falkovsky, "Optical properties of graphene," *J. Phys., Conf. Ser.*, vol. 129, no. 1, pp. 012004-1–012004-7, 2008.
[49] M. Aliofkhazraei, W. I. Milne, C. S. Ozkan, S. Mitura, J. L. Gervasoni, and N. Ali, *Graphene Science Handbook: Electrical and Optical Properties*. Boca Raton, FL, USA: CRC Press, 2016.
[50] P. Yeh, *Optical Waves in Layered Media*. New York, NY, USA: Wiley, 1988, ch. 6.
[51] T. Zhan, X. Shi, Y. Dai, X. Liu, and J. Zi, "Transfer matrix method for optics in graphene layers," *J. Phys., Condensed Matter*, vol. 25, no. 21, 2013, Art. no. 215301.
[52] Y. S. Jin, G. J. Kim, and S. G. Jeon, "Terahertz dielectric properties of polymers," *J. Korean Physical Soc.*, vol. 49, no. 2, pp. 513–517, 2006.
[53] I. V. Iorsh, I. S. Mukhin, I. V. Shadrivov, P. A. Belov, and Y. S. Kivshar, "Hyperbolic metamaterials based on multilayer graphene structures," *Phys. Rev. B*, vol. 87, 2013, Art. no. 075416.
[54] X. Wang, A. A. Belyanin, S. A. Crooker, D. M. Mittleman, and J. Kono, "Interference-induced terahertz transparency in a semiconductor magneto-plasma," *Nature Phys.*, vol. 6, no. 2, pp. 126–130, 2010.
[55] C. F. Hsieh, Y. C. Lai, R. P. Pan, and C. L. Pan, "Polarizing terahertz waves with nematic liquid crystals," *Opt. Lett.*, vol. 33, no. 11, pp. 1174–1176, 2008.
[56] W. Wenliangand Xiaohong, "Broadband and wide-angle terahertz wave polarizer based on symmetrical thin film structure," *Solid State Commun.*, vol. 169, pp. 28–31, 2013.